LETTERS

DNA-programmable nanoparticle crystallization

Sung Yong Park[1]*†, Abigail K. R. Lytton-Jean[1]*, Byeongdu Lee[2], Steven Weigand[3], George C. Schatz[1] & Chad A. Mirkin[1]

It was first shown[1,2] more than ten years ago that DNA oligonucleotides can be attached to gold nanoparticles rationally to direct the formation of larger assemblies. Since then, oligonucleotide-functionalized nanoparticles have been developed into powerful diagnostic tools[3,4] for nucleic acids and proteins, and into intracellular probes[5] and gene regulators[6]. In contrast, the conceptually simple yet powerful idea that functionalized nanoparticles might serve as basic building blocks that can be rationally assembled through programmable base-pairing interactions into highly ordered macroscopic materials remains poorly developed. So far, the approach has mainly resulted in polymerization, with modest control over the placement of, the periodicity in, and the distance between particles within the assembled material. That is, most of the materials obtained thus far are best classified as amorphous polymers[7–16], although a few examples of colloidal crystal formation exist[8,16]. Here, we demonstrate that DNA can be used to control the crystallization of nanoparticle–oligonucleotide conjugates to the extent that different DNA sequences guide the assembly of the same type of inorganic nanoparticle into different crystalline states. We show that the choice of DNA sequences attached to the nanoparticle building blocks, the DNA linking molecules and the absence or presence of a non-bonding single-base flexor can be adjusted so that gold nanoparticles assemble into micrometre-sized face-centred-cubic or body-centred-cubic crystal structures. Our findings thus clearly demonstrate that synthetically programmable colloidal crystallization is possible, and that a single-component system can be directed to form different structures.

From a surface receptor standpoint, gold nanoparticles can be programmed to behave as a single-component or binary system by using the sequence-specific recognition properties of DNA (Fig. 1a) and designing DNA linkers with two different regions (Fig. 1b and c). In a typical experiment, gold nanoparticles (15 nm in diameter) are modified with synthetic oligonucleotides[17] and then linker DNA is introduced; the latter contains a region 1 complementary to the

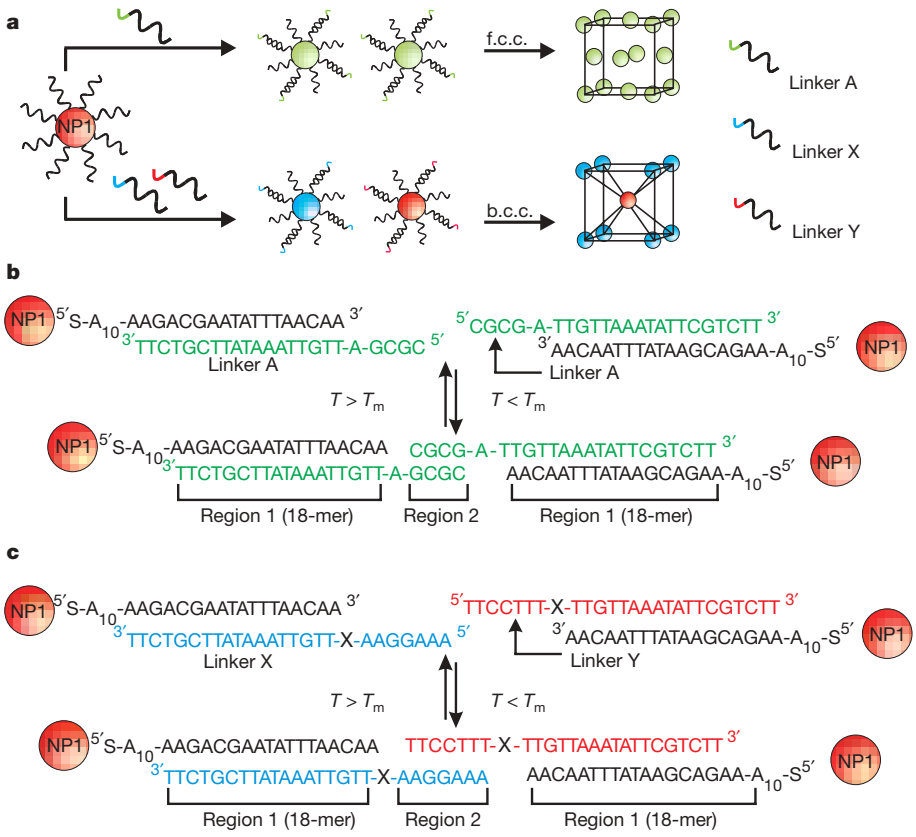

Figure 1 | Scheme of gold nanoparticle assembly method. a, Gold nanoparticle–DNA conjugates can be programmed to assemble into different crystallographic arrangements by changing the sequence of the DNA linkers. **b**, Single-component assembly system (f.c.c.) where gold nanoparticles are assembled using one DNA sequence, linker-A. **c**, Binary-component assembly system (b.c.c.) in which gold nanoparticles are assembled using two different DNA linkers -X and -Y. X in the DNA sequence denotes the flexor region: A, PEG_6 or no base. NP1 indicates that the same gold nanoparticle-DNA conjugates were used in all experiments.

[1]Department of Chemistry and International Institute for Nanotechnology, Northwestern University, 2145 Sheridan Road, Evanston, Illinois 60208-3113, USA. [2]X-ray Science Division, Advanced Photon Source, Argonne National Laboratory. [3]DND-CAT Synchrotron Research Center, Northwestern University, APS/ANL 432-A004, 9700 S. Cass Avenue, Argonne, Illinois 60439, USA. †Present address: Department of Biostatistics and Computational Biology, University of Rochester, 601 Elmwood Avenue, Rochester, New York 14642, USA. *These authors contributed equally to this work.

gold-nanoparticle-bound DNA, and a region 2 that acts as a dangling end and can be varied to control the interactions between the gold nanoparticles. In all cases, region 1 is significantly longer than region 2, and therefore the duplex formed from hybridization with region 1 is more stable than the duplex formed from hybridization with region 2. This allows region 2 to be thermally addressable without significantly perturbing region 1 (ref. 18). By designing a linker sequence in which region 2 is self-complementary, the nanoparticles will effectively behave as a single-component system (Fig. 1b). Alternatively, by designing a linker with a non-self-complementary region 2, an additional, different linker is required to achieve particle assembly (Fig. 1c). From a surface receptor standpoint, the latter design creates a binary system in which gold nanoparticles hybridized to linker-X (AuNP-X) can only bind to gold nanoparticles hybridized to linker-Y (AuNP-Y). Between region 1 and 2, a non-binding single DNA base, called a flexor, is added (typically adenosine, A). As discussed later, the flexor plays a crucial role in DNA-programmable nanoparticle crystallization.

The ability to simulate a single-component or binary system without the irreversible chemical alteration of the gold nanoparticle–oligonucleotide conjugate is a unique aspect of this system. From an energy minimization standpoint, it is expected that the gold nanoparticle assemblies will maximize the number of hybridized DNA linkages by adopting a conformation that will maximize the number of nanoparticle nearest neighbours. In a single-component system, in which each particle can bind to every other particle with equal affinity, a close-packed face-centred-cubic (f.c.c.) structure is expected to form wherein each particle has 12 nearest neighbours. Alternatively, in a binary system, where AuNP-X can bind only to AuNP-Y, the maximum number of hybridization events is achieved in a non-close-packed body-centred-cubic (b.c.c.) structure wherein each particle has eight nearest neighbours (that is, a caesium chloride lattice). Should a binary system assemble into a close-packed structure, each particle will have, on average, less than eight compatible nearest neighbours through which DNA hybridization can occur (see also Supplementary Information).

We begin by demonstrating the ability to form close-packed macroscopic single-crystalline domains using the single-component nanoparticle system (Fig. 1b). To create a well-defined and close-packed crystal, weak and reversible interactions are necessary[13,19–23]. This is achieved by combining the gold nanoparticles and linker-A above the melting temperature (T_m) of region 2 (~44 °C) followed by slow cooling (10 min/1 °C) to room temperature, to ensure that crystal formation is thermodynamically and not kinetically controlled. Two-dimensional small-angle X-ray scattering (SAXS) data collected from the resultant particle assemblies display a scattering pattern specific to a f.c.c. structure (Fig. 2a). In addition to well-defined scattering rings, individual scattering spots are clearly seen in the first and second ring indicating the formation of many large crystallites (Fig. 2b).

The majority of the high-intensity spots reside in the first ring and display nearly identical q values. The two-dimensional data were integrated and normalized based on the q value from the first ring (red line in Fig. 2c). The normalized spot positions were located at $q/q_0 \approx 1$, $\sqrt{4/3}$, $\sqrt{8/3}$, $\sqrt{11/3}$ and 2, identifying the crystalline domains as possessing f.c.c. structure when compared to the theoretical spectrum (green line in Fig. 2c). Indeed, the averaged structure factor $S(q)$ (red line in Fig. 2c) is very similar to a theoretical simulation (blue line in Fig. 2c) of the SAXS pattern for a f.c.c. configuration containing a small amount of disorder[24] (Supplementary Information). We note that the experimental data exhibit a small feature at $q/q_0 = \sqrt{3}$, which could be due to a hexagonal close-packed crystalline domain, a compressed f.c.c. crystalline domain, or a less ordered random hexagonal close-packed domain. However, the dominant overall structure is clearly f.c.c. We use the Scherrer formula[25] to estimate from the spots in the scattering pattern a size of around 2.1 μm (~10^6 particles) for the single-crystal domains. The average interparticle distance can also be determined from the position of the first peak, which in q space is placed at $\sqrt{6}\pi/d_{Au}$, where d_{Au} is the distance between the nanoparticle centres. This gives a measured interparticle distance of 27.9 nm, which falls within the range of the predicted interparticle distance (28.6–36.1 nm) that is based on the length of the DNA linkers (Supplementary Information).

More interesting than the formation of a close-packed structure is the ability to program the assembly of the same nanoparticles into a non-close-packed structure. This was achieved by using linkers -X and -Y, to create a binary system (from the surface receptor standpoint) which drives the gold nanoparticle assembly into a non-close-packed b.c.c. structure to maximize the number of DNA hybridization events (Fig. 1c). The two-dimensional SAXS pattern for this system clearly indicates a b.c.c. structure (Fig. 3a and b). The averaged $S(q)$, determined by integration and normalization based on the q value from the first ring, shows five peak positions at $q/q_0 = 1$, $\sqrt{2}$, $\sqrt{3}$, 2 and $\sqrt{5}$, in agreement with the theoretical b.c.c. structure (green line in Fig. 3b). In addition to the peak

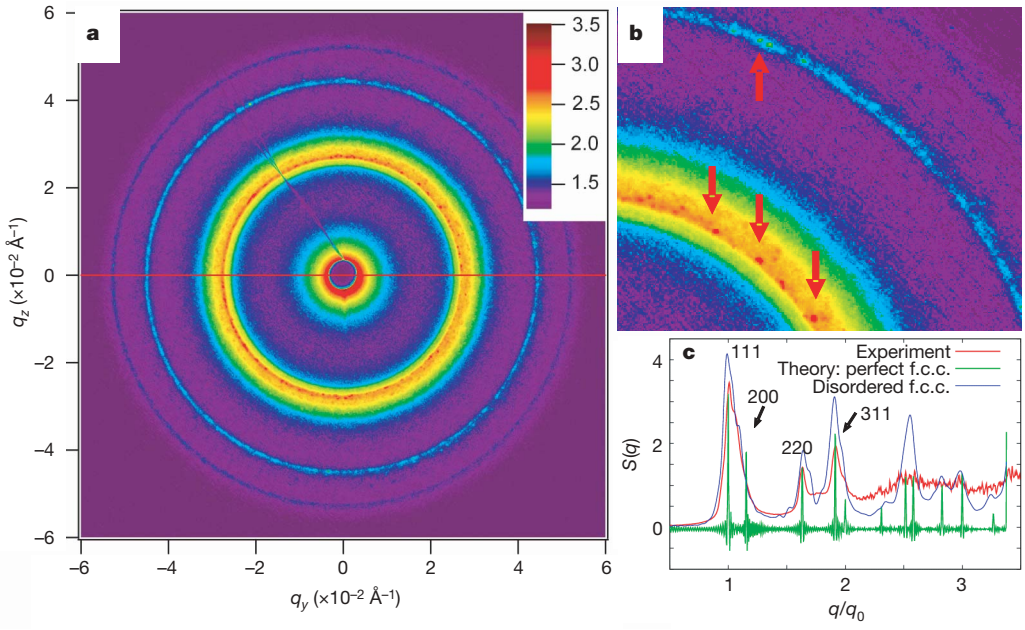

Figure 2 | f.c.c. gold nanoparticle SAXS pattern. **a**, SAXS pattern of micrometre-size single-crystalline domains using a single-component system. The colour scale indicates the intensity, I. The image is in log scale. **b**, A partial magnification of **a** displays individual spots of increased scattering intensity (red arrows). **c**, The integrated data from **a** shows an f.c.c. crystal structure. The x-axis is normalized to the first peak from **a** (2.76×10^{-2} Å^{-1}). The entire spectrum from **c** is not shown in **a**.

position, the relative peak heights are consistent with the theoretical calculations. Using the Scherrer formula, the average size of a single-crystalline domain was estimated to be about 600 nm ($\sim 10^4$ particles) with an average *d*-spacing of 31 nm (estimated range 29.6–37.1 nm; Supplementary Information).

The binary system discussed above can also form a close-packed structure, by carefully controlling the temperature at which AuNP-X and AuNP-Y are combined. If the binary particles are treated in the same manner as the single-component system by combining AuNP-X and AuNP-Y above the T_m of region 2 (weak DNA attractive forces) followed by slow cooling, a substitutionally disordered f.c.c. structure[21] is formed, which presents an f.c.c. scattering pattern (Supplementary Information). Alternatively, a non-close-packed b.c.c. structure is achieved by combining AuNP-X and AuNP-Y at room temperature, below the T_m ($\sim 37\,^{\circ}C$) of region 2 (stronger DNA attractive forces) followed by annealing a few degrees below the T_m.

The formation of the different crystal structures is attributed to a competition between the entropic and enthalpic contributions involved in the assembly process at different temperatures. From an entropic standpoint, a close-packed structure is favoured over a non-close-packed structure because the entropy of the entire system can be maximized if the aggregates possess the smallest possible volume fraction[22,26]. Therefore, if gold nanoparticles begin to assemble near the DNA T_m, where the DNA binding strength is very weak and the enthalpic contribution is small, the entropic contribution will dominate the assembly process and a close-packed structure forms. However, if the gold nanoparticles are combined several degrees below the T_m, the enthalpic contribution associated with DNA hybridization will govern the assembly process and a non-close-packed structure forms that maximizes the number of DNA hybridization events.

Gold nanoparticle–oligonucleotide conjugate systems have many variables that can be adjusted to affect the final structure. In addition to the DNA sequence as addressed above, DNA rigidity, DNA length and particle size can be manipulated to influence gold nanoparticle crystallization without changing the basic properties of the overall system. To probe the importance of these variables in the crystallization process, we began by changing the rigidity of the flexor region which is not involved in the DNA hybridization. Two variations of linker-X and -Y DNA were synthesized; one without the A-flexor and one with a polyethylene glycol oligomer (PEG_6) in place of the A-flexor (Fig. 1c). The absence of the A-flexor should result in a rigid system while the PEG_6-flexor should give a more flexible system. The first peak in the SAXS pattern from the sample with the PEG_6-flexor is the sharpest, and the sample with no flexor is the broadest, Fig. 3c. This indicates that the sample with the flexible PEG_6-flexor can grow larger crystals. Also, after similar crystallization times, a more well-defined crystalline structure arises from the PEG_6-flexor (Fig. 3d). Hence, greater flexibility can enhance the assembly process and results in a more well-defined crystalline structure.

Next, the effect of DNA length was interrogated by designing a gold nanoparticle with a shorter DNA sequence in region 1 (12-mer versus 18-mer in Fig. 4a) while maintaining an elevated T_m compared to region 2. When both AuNP-X and AuNP-Y contain the shorter region 1 DNA sequence, the result is a b.c.c. structure, similar to before, only with a shorter interparticle distance. However, the combination of a short region 1 AuNP-X and a long region 1 AuNP-Y (Fig. 4b), results in a b.c.c. structure that is thermally more stable (Supplementary Information). This suggests that the aspect ratio between the effective radii of the binary DNA-linked gold nanoparticles is an important factor in the crystallization process. As the aspect ratio of the particles decreases from one, a b.c.c. structure becomes entropically more favoured because the volume fraction of the b.c.c. structure is reduced[22,26] and the f.c.c. structure loses its entropic advantage as the particles become effectively polydisperse[27]. This was further addressed by using small gold nanoparticles (10 nm) with a short region 1 and large gold nanoparticles (15 nm) with a long

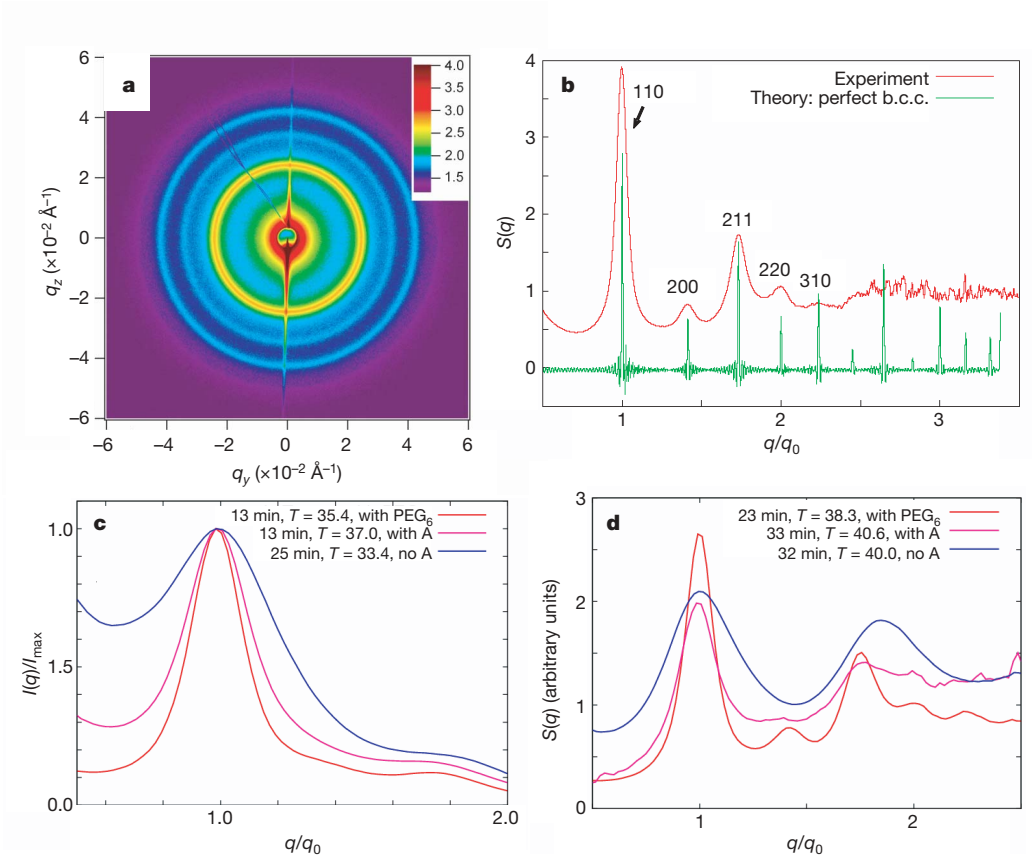

Figure 3 | b.c.c. gold nanoparticle SAXS pattern. **a**, SAXS pattern of the binary gold nanoparticle system combined below the T_m of region 2. The colour scale indicates the intensity, *I*. The image is in log scale. **b**, The integrated SAXS data from **a** shows a b.c.c. crystal structure. **c**, Comparison of the first peak between three different binary samples containing different flexor regions as assembly is initiated. **d**, Comparison of the entire SAXS pattern of three different binary samples containing different flexors (A, PEG_6, no flexor). The times given indicate the time passed since the initiation of the experiment.

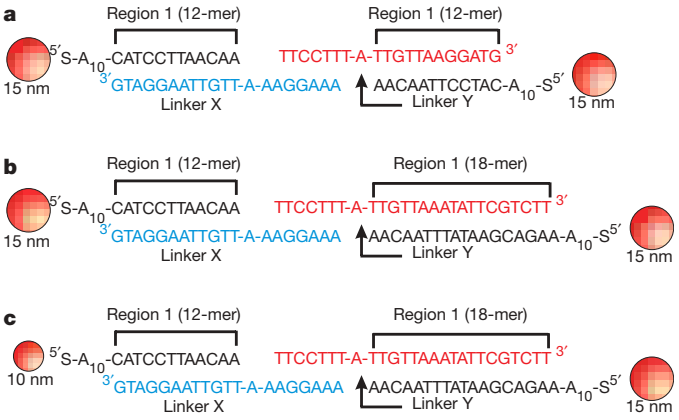

Figure 4 | Changing DNA length and gold nanoparticle size in the binary-component assembly scheme (b.c.c.). a, Both AuNP-X and AuNP-Y contain a shorter DNA length in region 1: 12-mer versus 18-mer from Fig. 1. **b**, Asymmetric binary gold nanoparticle assembly in which AuNP-X contains a short 12-mer region 1 and AuNP-Y contains a long 18-mer region 1. **c**, Asymmetric binary gold nanoparticle assembly in which AuNP-X in **b** is a small 10 nm gold nanoparticle and AuNP-Y is a larger 15 nm gold nanoparticle.

region 1 (Fig. 4c). These samples formed crystals with a b.c.c. structure that exhibit even greater stability, such that the b.c.c. structure can be achieved independent of pathway (that is, slow cooling from above T_m versus combining and annealing below T_m) (Supplementary Information).

In all cases, to create well-defined programmable crystalline structures using DNA-linked gold nanoparticles, several conditions must be met. In addition to having control over the strength of the DNA attractive forces, it is important to have highly monodisperse particles (<10%). As shown in a dissipative particle dynamics (DPD) simulation[28,29], particles with a polydispersity of 20% do not form well-defined crystalline assemblies, which is in accordance with our experiments (Supplementary Information). Therefore, all crystalline structures presented in this report were obtained using nanoparticles with polydispersity less than 10%.

These findings demonstrate that DNA-directed assembly affords powerful and versatile control over the formation of colloidal nanoparticle crystals. We expect that as advances in building valency into nanoparticle structures through edge- and face-selective modification processes mature[18,30], the number and type of crystalline structures accessible through this approach should significantly increase.

Received 23 October; accepted 28 November 2007.

1. Mirkin, C. A., Letsinger, R. L., Mucic, R. C. & Storhoff, J. J. A DNA-based method for rationally assembling nanoparticles into macroscopic materials. *Nature* **382,** 607–609 (1996).
2. Alivisatos, A. P. *et al.* Organization of 'nanocrystal molecules' using DNA. *Nature* **382,** 609–611 (1996).
3. Rosi, N. L. & Mirkin, C. A. Nanostructures in biodiagnostics. *Chem. Rev.* **105,** 1547–1562 (2005).
4. Ozin, G. A. & Arsenault, A. C. *Nanochemistry: A Chemical Approach to Nanomaterials* (Royal Society of Chemistry, Cambridge, UK, 2005).
5. Seferos, D. S., Giljohann, D. A., Hill, H. D., Prigodich, A. E. & Mirkin, C. A. Nano-flares: Probes for transfection and mRNA detection in living cells. *J. Am. Chem. Soc.* **129,** 15477–15479 (2007).
6. Rosi, N. L. *et al.* Oligonucleotide-modified gold nanoparticles for intracellular gene regulation. *Science* **312,** 1027–1030 (2006).
7. Park, S. J., Lazarides, A. A., Storhoff, J. J., Pesce, L. & Mirkin, C. A. The structural characterization of oligonucleotide-modified gold nanoparticle networks formed by DNA hybridization. *J. Phys. Chem. B* **108,** 12375–12380 (2004).
8. Biancaniello, P. L., Kim, A. J. & Crocker, J. C. Colloidal interactions and self-assembly using DNA hybridization. *Phys. Rev. Lett.* **94,** 058302 (2005).
9. Park, S. J., Lazarides, A. A., Mirkin, C. A. & Letsinger, R. L. Directed assembly of periodic materials from protein and oligonucleotide-modified nanoparticle building blocks. *Angew. Chem. Int. Edn* **40,** 2909–2912 (2001).
10. Park, S. Y. & Stroud, D. Theory of melting and the optical properties of gold/DNA nanocomposites. *Phys. Rev. B* **67,** 212202 (2003).
11. Park, S. Y. & Stroud, D. Structure formation, melting, and optical properties of gold/DNA nanocomposites: Effects of relaxation time. *Phys. Rev. B* **68,** 224201 (2003).
12. Park, S. Y., Lee, J. S., Georganopoulou, D., Mirkin, C. A. & Schatz, G. C. Structures of DNA-linked nanoparticle aggregates. *J. Phys. Chem. B* **110,** 12673–12681 (2006).
13. Velev, O. D. Self-assembly of unusual nanoparticle crystals. *Science* **312,** 376–377 (2006).
14. Strable, E., Johnson, J. E. & Finn, M. G. Natural nanochemical building blocks: icosahedral virus particles organized by attached oligonucleotides. *Nano Lett.* **4,** 1385–1389 (2004).
15. Nykypanchuk, D., Maye, M. M., der Lelie, D. & Gang, O. DNA-based approach for interparticle interaction control. *Langmuir* **23,** 6305–6314 (2007).
16. Kim, A. J., Biancaniello, P. L. & Crocker, J. C. Engineering DNA-mediated colloidal crystallization. *Langmuir* **22,** 1991–2001 (2001).
17. Hurst, S. J., Lytton-Jean, A. K. R. & Mirkin, C. A. Maximizing DNA loading on a range of gold nanoparticle sizes. *Anal. Chem.* **78,** 8313–8318 (2006).
18. Huo, F., Lytton-Jean, A. K. R. & Mirkin, C. A. Asymmetric functionalization of nanoparticles based on thermally addressable DNA interconnects. *Adv. Mat.* **18,** 2304–2306 (2006).
19. Redl, F. X., Cho, K. S., Murray, C. B. & O'Brien, S. Three-dimensional binary superlattices of magnetic nanocrystals and semiconductor quantum dots. *Nature* **423,** 968–971 (2003).
20. Leunissen, M. E. *et al.* Ionic colloidal crystals of oppositely charged particles. *Nature* **437,** 235–240 (2005).
21. Bartlett, P. & Campbell, A. I. Three-dimensional binary superlattices of oppositely charged colloids. *Phys. Rev. Lett.* **95,** 128302 (2005).
22. Shevchenko, E. V., Talapin, D. V., Kotov, N. A., O'Brien, S. & Murray, C. B. Structural diversity in binary nanoparticle superlattices. *Nature* **439,** 55–59 (2006).
23. Kalsin, A. M. *et al.* Electrostatic self-assembly of binary nanoparticle crystals with a diamond-like lattice. *Science* **312,** 420–424 (2006).
24. Donev, A., Torquato, S., Stillinger, F. H. & Connelly, R. A linear programming algorithm to test for jamming in hard-sphere packings. *J. Comput. Phys.* **197,** 139–166 (2004).
25. Cullity, B. D. *Elements of X-Ray Diffraction* (Addison-Wesley, Reading, Massachusetts, 1978).
26. Frenkel, D. Colloidal crystals: plenty of room at the top. *Nature Mater.* **5,** 85–86 (2006).
27. Kiely, C. J., Fink, J., Brust, M., Bethell, D. & Schiffrin, D. J. Spontaneous ordering of bimodal ensembles of nanoscopic gold clusters. *Nature* **396,** 444–446 (1998).
28. Hoogerbrugge, P. J. & Koelman, J. M. V. A. Simulating microscopic hydrodynamic phenomena with dissipative particle dynamics. *Europhys. Lett.* **19,** 155–160 (1992).
29. Español, P. & Warren, P. Statistical mechanics of dissipative particle dynamics. *Europhys. Lett.* **30,** 191–196 (1995).
30. Xu, X.-Y., Rosi, N. L., Wang, Y., Huo, F. & Mirkin, C. A. Asymmetric functionalization of gold nanoparticles with oligonucleotides. *J. Am. Chem. Soc.* **128,** 9286–9287 (2006).

Supplementary Information is linked to the online version of the paper at www.nature.com/nature.

Acknowledgements C.A.M. acknowledges the AFOSR and NSF for support of this work. C.A.M is also grateful for a NIH Director's Pioneer Award. S.Y.P. and G.C.S. were supported by the NSF. S.Y.P. and G.C.S. thank S. Torquato for providing numerical model output and S. Ryu for discussions. We thank S. Seifert for help with the SAXS set-up. We thank the Argonne National Laboratory for the use of the APS, supported by the US Department of Energy, Office of Science, Office of Basic Energy Sciences.

Author Contributions C.A.M. was the originator of the concept of programmable colloidal crystallization with DNA. A.K.R.L.-J. and C.A.M were responsible for the synthetic components of the project and sequence design. S.Y.P. and G.C.S. were responsible for the theoretical components of the project. S.W. designed the SAXS set-up. S.Y.P., A.K.R.L.-J. and B.L. designed and performed SAXS experiments. S.Y.P. and B.L. analysed the SAXS data. All authors contributed to the writing of the manuscript.

Author Information Reprints and permissions information is available at www.nature.com/reprints. Correspondence and requests for materials should be addressed to C.A.M. (chadnano@northwestern.edu).